International Journal of Infrared and Millimeter Waves, Vol. 21, No. 11, 2000

TRACES OF STOCHASTICITY IN ELECTRON TRAJECTORIES IN GYROTRON RESONATORS

M. I. Airila,[1] O. Dumbrajs,[1] A. Reinfelds,[2] and D. Teychenné[1]

[1]*Department of Engineering Physics and Mathematics*
Helsinki University of Technology
FIN-02150 Espoo, Finland
[2]*Institute of Mathematics*
Latvian Academy of Sciences and University of Latvia
LV-1524 Riga, Latvia

Received August 24, 2000

Abstract

The Hamiltonian approach is used to analyze the equation describing the electron interaction in gyrotron resonators with realistic RF field profiles. A detailed numerical study of the behavior of electron trajectories for some specific values of parameters controlling the interaction is performed. It is found that in some cases chaos-like motions of electrons are possible.

Key words: Gyrotron, stochasticity

I. Introduction

Gyrotron is a special tube generating powerful radio waves in the millimeter wave range. Gyrotrons are mainly used to heat nuclear fusion plasma, in order to induce controlled thermonuclear reactions on earth. In addition, they have found a wide utility in radars and the high-temperature processing of materials. Extensive literature exists on various experimental and theoretical aspects of these microwave tubes [1]. However until recently no fundamental mathematical analysis of the basic equation describing the electron interaction with the RF field in gyrotron resonators was available. The first analysis of this kind was presented in [2] where it was proven that in the case when the RF field is represented by a Gaussian-type function, the solutions of the gyrotron equation are asymptotically equal to the solutions of the corresponding unforced equation. This means that chaos, which, in principle, can develop in a resonator for some values of control parameters, can be only transient, i.e., electrons again follow regular trajectories once they leave the interaction space. In [3] this analysis was extended to the case

0195-9271/00/1100-1759$18.00/0

of an infinitely long resonator in which the RF field was represented by a propagating wave. It was shown that in this case phase trajectories of the electrons are much more complicated than in the case of a decaying RF field. The analysis in these two papers was based on the theory of differential equations and, possibly, was not easily understandable for a physically oriented reader. In the present work we employ the powerful and physically transparent Hamiltonian method used recently [4] in analyzing chaos in a gyrotron-type of interaction. We include in the analysis a completely realistic case: a resonator with a finite length and a true longitudinal distribution of the RF field.

II. Gyrotron equations

The equation which describes the electron motion in a gyrotron resonator can be written as follows [5]:

$$\frac{dp}{d\zeta} + i(\Delta + |p|^2 - 1)p = if(\zeta)F \tag{1}$$

with the initial condition $p(\zeta_0) = \exp(i\theta_0)$, where $0 \leq \theta_0 < 2\pi$. Here p is the dimensionless transverse momentum of the electron, $\zeta = \frac{\beta_{\perp 0}^2 \omega}{2\beta_{\|0} c} \cdot z$ is the dimensionless coordinate, $\beta_{\perp 0} = v_{\perp 0}/c$ and $\beta_{\|0} = v_{\|0}/c$ are the normalized transverse and parallel velocities of the electron at the entrance to the cavity, $\Delta = \frac{2(\omega - \omega_c)}{\beta_{\perp 0}^2 \omega}$ is the frequency mismatch, $\omega_c = 56\pi B/\gamma_{rel}$ is the electron cyclotron frequency in GHz, B is the magnetic field in Tesla, $\gamma_{rel} = 1 + U/511$ is the relativistic factor, U is the accelerating voltage in kV. The dimensionless electron beam to RF coupling factor F is given by the expression:

$$F = \sqrt{0.00047 Q_{dif} P_{out} \frac{J_{m\pm1}^2\left(\frac{2\pi}{\lambda} R_{el}\right)}{\gamma_{rel} U \eta_{el} \beta_{\|0} \beta_{\perp 0}^2 (\nu^2 - m^2) J_m^2(\nu) \int_0^{\zeta_{out}} |f(\zeta)|^2 d\zeta}},$$

where Q_{dif} is the diffractive quality factor of the cavity, P_{out} is the output power of a gyrotron in kW, J is the Bessel function, λ is the wave length, ν is the eigenvalue, R_{el} is the electron beam radius, and $\pm$ indicate the two possible directions of rotation of RF field (co-rotating with the electrons $-$, and counter-rotating with the electrons $+$). The electron efficiency is $\eta_{el} = \frac{\alpha^2}{1+\alpha^2} \cdot \eta_\perp$, where $\eta_\perp$ is perpendicular efficiency:

$$\eta_\perp = 1 - \frac{1}{2\pi} \int_0^{2\pi} |p(\zeta_{out})|^2 d\vartheta_0$$

and $\alpha = \beta_\perp/\beta_\|$ is the pitch factor of the electrons.

Equation (1) represents the so-called cold-cavity approximation in the gyrotron theory when the RF field in a gyrotron resonator $f(\zeta)$ depends only on the

geometry of the resonator, but not on the electron motion, i.e., f does not depend on p. In this case the RF field in a cavity is usually approximated by a Gaussian

$$f(\zeta) = \exp\left[-\left(\frac{2\zeta}{\mu} - \sqrt{3}\right)^2\right] \tag{2}$$

where $\mu = \pi\left(\frac{\beta_\perp^2}{\beta_\parallel}\right)\frac{L}{\lambda}$ is the dimensionless length of the resonator with length L. In [2] equation (1) was examined in detail from the mathematical point of view. In particular electron trajectories were classified and the asymptotical equivalence of (1) and of the corresponding unforced equation ($f(\zeta) \equiv 0$)

$$\frac{dq}{d\zeta} + i(\Delta + |q|^2 - 1)q = 0, \quad q(\zeta_0) = q_0. \tag{3}$$

was proved in the case when the function $f(\zeta)$ decays fast enough for large ζ: faster than $1/\zeta^{2+\epsilon}$. In such a case each solution of (1) corresponds to a solution of (3) with changed initial data. It should be emphasized that the RF field in the cavity represented by a Gaussian (2) is an approximation which is valid in resonators with very high quality factors. In realistic cases even in the cold-cavity approximation $f(\zeta)$ has to be determined for each specific resonator geometry by solving the following second-order differential equation:

$$\frac{d^2 f}{d\zeta^2} + \gamma(\zeta)^2 f = 0 \tag{4}$$

with the boundary conditions

$$\frac{df}{d\zeta} = i\gamma(\zeta)f, \quad \zeta = 0,$$

$$\frac{df}{d\zeta} = -i\gamma(\zeta)f, \quad \zeta = \zeta_{out}$$

Here the function $\gamma(\zeta)$ depends on the frequency of oscillations, the quality factor and the geometry of the resonator. For the purpose of the present study we can simply write $\gamma(\zeta) = k(\zeta) + i\kappa(\zeta)$. In Figs. 1 and 2 we show typical examples of $f(\zeta)$ and $\gamma(\zeta)$.

As is evident from these figures, for $\zeta \geq 70$ where the output taper of the cavity goes over into cylinder the function $f(\zeta)$ can be approximated as a wave moving in the $+\zeta$ direction: $f(\zeta) \sim e^{-i\gamma\zeta}$. Moreover, since $k \gg \kappa$, one can write $f(\zeta) \sim e^{-ik\zeta}$.

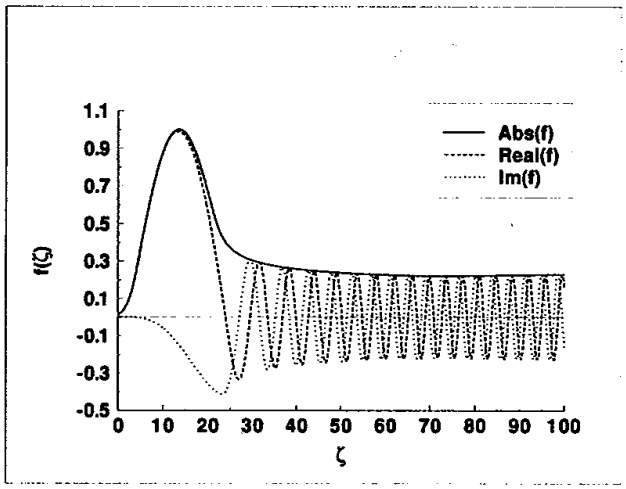

Figure 1: The longitudinal profile of the RF field in a realistic gyrotron resonator corresponding to $\mu \approx 9$.

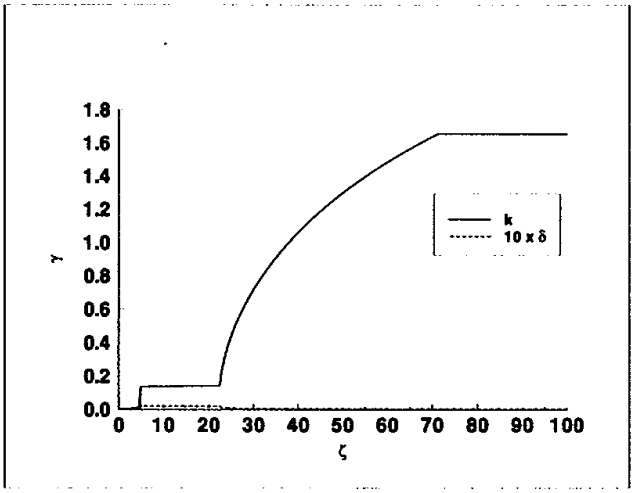

Figure 2: The function $\gamma(\zeta)$.

III. Hamiltonian method

By introducing the notation $p = Q + iP$ in (1), we obtain the dynamical system:

$$\begin{cases} \dfrac{dQ}{d\zeta} = \dfrac{\partial H}{\partial P} = & -\delta P + P(Q^2 + P^2) - Fg(\zeta) \\ \dfrac{dP}{d\zeta} = -\dfrac{\partial H}{\partial Q} = & +\delta Q - Q(Q^2 + P^2) + Fh(\zeta) \end{cases} \tag{5}$$

where $\delta = 1 - \Delta$, $g(\zeta)$ and $h(\zeta)$ are respectively the imaginary and real part of $f(\zeta)$. The dimensionless coordinate ζ can be regarded as time and the time-dependent Hamiltonian with one degree of freedom can be written as:

$$\begin{aligned} &H(Q,P,\zeta) = H_0 + H_1 = -\frac{\delta}{2}(Q^2 + P^2) + \\ &\tfrac{1}{4}(Q^2 + P^2)^2 - F(Qh(\zeta) + Pg(\zeta)) \end{aligned} \tag{6}$$

The unperturbed Hamiltonian is integrable and is defined as follows:

$$H_0(Q,P,\zeta) = -\frac{\delta}{2}(Q^2 + P^2) + \frac{1}{4}(Q^2 + P^2)^2 = E_0 \tag{7}$$

where E_0 is the total energy which is conserved during the evolution of the system (the Hamiltonian system). The term $H_1 = -F(Qh(\zeta) + Pg(\zeta))$ represents the driving force and is considered as a perturbation.

In general in Hamiltonian methods we first analyze the unperturbed part to determine the important properties of the system (constants of motion). Subsequently the nonlinear part of the Hamiltonian is studied by the perturbative approach (almost integrable). We now can analyze different solutions either by means of the Poincaré sections, or in terms of the angle-action variables. The first approach is a powerful tool for detection of chaotic solutions. The second approach allows one to analyze the fundamental properties of the dynamical system and to find the elliptic and hyperbolic points (fixed points). Knowing these points we can understand the structure of the phase space. Namely, hyperbolic points play a crucial role in the possible emerging of chaos around them as a result of the Kolmogorov-Arnold-Moser (KAM) torus destruction by the perturbation associated with the nonlinear part of the Hamiltonian. In this case some constants of motion are destroyed. The angle-action variables allow us in some cases to separate the variables in the Hamiltonian, to find the invariants (constants of motion), and to demonstrate the integrability of the dynamical system.

We now rewrite the Hamiltonian H_0 in terms of the angle-action variables

(θ, J). We use for this the canonical transformation $(Q, P) \longrightarrow (\theta, J)$ which provides $H_0(Q, P) \longrightarrow \overline{H}_0(J)$. The action J is defined as:

$$J = \frac{1}{2\pi} \oint_0^{2\pi} P dQ \tag{8}$$

From (7) we obtain the momentum $P = \sqrt{\sqrt{4E_0 + \delta^2} + \delta - Q^2}$ and the coordinate $Q \in [-Q_M, Q_M]$, where $Q_M = \sqrt{\delta + \sqrt{4E_0 + \delta^2}}$. Now the action J becomes:

$$\begin{aligned} J = 4 \times \frac{1}{2\pi} \int_0^{Q_M} \sqrt{\sqrt{4E_0 + \delta^2} + \delta - Q^2}\, dQ = \\ \frac{1}{2}(\delta + \sqrt{4E_0 + \delta^2}) \end{aligned} \tag{9}$$

This is the first integral of motion (constant of motion) for the unperturbed Hamiltonian system. Substituting now E_0 in terms of the momentum P into (9) we obtain:

$$P = \sqrt{2J - Q^2} \tag{10}$$

We now can calculate the angle θ by means of the canonical transformation which is defined as: $P = \dfrac{\partial S}{\partial Q}$ and $\theta = \dfrac{\partial S}{\partial J}$ where $S(J, Q)$ is the generating function. The expression for the Hamiltonian in terms of the action J is obtained from the Hamilton-Jacobi equation:

$$H_0(\frac{\partial S}{\partial Q}, Q) = \overline{H}_0(J) = E_0 \tag{11}$$

With the help of (9) the Hamiltonian $\overline{H}_0(J)$ writes:

$$\overline{H}_0(J) = J^2 - \delta J \tag{12}$$

The Hamilton equations immediately lead to the following system of equations:

$$\begin{cases} \dot{J} = -\dfrac{\partial \overline{H}_0}{\partial \theta} = 0 \Longrightarrow J = const. \\ \dot{\theta} = \dfrac{\partial \overline{H}_0}{\partial J} = \omega_\theta = 2J - \delta \end{cases}$$

From here it follows that the period of motion is $T = \dfrac{2\pi}{\omega_\theta} = \dfrac{2\pi}{2J - \delta}$. The generating function $S(J, Q)$ depends only on the coordinate Q, because the action J is the constant of motion. From this and from the canonical transformation we obtain:

$$S(J, Q) = \int_0^Q P dQ = \int_0^Q \sqrt{2J - Q^2} dQ \tag{13}$$

For the angle θ we can now write:

$$\theta = \frac{\partial S(J,Q)}{\partial J} = \int_0^Q \frac{\partial}{\partial J}\left(\sqrt{2J - Q^2}\right) dQ \tag{14}$$

Carrying out the integration, we finally find for the angle θ the expression:

$$\theta = \arcsin \frac{Q}{\sqrt{2J}} \tag{15}$$

From (10) and (15) we have also:

$$\begin{cases} Q = \sqrt{2J}\sin\theta \\ P = \sqrt{2J}\cos\theta \end{cases} \tag{16}$$

This system gives the transformation from the action-angle variables to the original variables Q and P. The period of the unperturbed dynamical system in the old variables becomes $T = 2\pi(Q_0^2 + P_0^2 - (1-\Delta))^{-1}$, where Q_0^2 and P_0^2 are the initial conditions. The trajectories of the electrons are circles with the radius $\sqrt{Q_0^2 + P_0^2}$ and are centered at the origin in agreement with what was found in [2].

We now can write the total Hamiltonian (6) as a function of the angle-action variables as follows: $\overline{H}(J,\theta,\zeta) = \overline{H}_0(J) + \overline{H}_1(J,\theta,\zeta)$. With the system (16) we obtain:

$$\overline{H}(J,\theta,\zeta) = J^2 - \delta J - F\sqrt{2J}\,[h(\zeta)\sin\theta + g(\zeta)\cos\theta] \tag{17}$$

This is still a time-dependent Hamiltonian with one degree of freedom. The nonlinear part $\overline{H}_1$ of the Hamiltonian (17) couples through $f(\zeta)$ the action J and the angle θ and perturbs the integrable Hamiltonian $\overline{H}_0$. In a general case the total Hamiltonian $\overline{H}$ becomes non-integrable. It can exhibit a complex behavior and also can lead to chaotic solutions.

A. Infinitely long idealized resonator

The solutions of (17) depend on the functions $h(\zeta)$ and $g(\zeta)$. As noted already in Sec. II the real and imaginary part of $f(\zeta)$ for large values of ζ can be represented as periodic functions with period k: $h(\zeta) \sim \cos(k\zeta)$ and $g(\zeta) \sim \sin(k\zeta)$. Assuming that an idealized resonator is such that this representation is valid in the entire interaction volume, we can rewrite the Hamiltonian (17) as follows:

$$\overline{H}(J,\theta,\zeta) = (J^2 - \delta J) - F\sqrt{2J}\,\sin(\theta + k\zeta)$$

It is possible to eliminate the explicit time dependence by means of a new generating function [6] $F_2(I,\theta) = I\,(\theta + k\zeta)$. The canonical transformation gives for the new variables (ψ, I) the system:

$$\begin{cases} J = \dfrac{\partial F_2}{\partial \theta} \Longrightarrow J = I \\ \psi = \dfrac{\partial F_2}{\partial I} \Longrightarrow \psi = \theta + k\zeta \end{cases}$$

The new Hamiltonian must satisfy the equation:

$$\overline{H'}(I,\psi) = \overline{H}(J,\theta,\zeta) + \frac{\partial F_2}{\partial \zeta}.$$

We finally obtain the time-independent Hamiltonian

$$\overline{H'}(I,\psi) = (I^2 - I\,(\delta - k)) - F\sqrt{2I}\,\sin\psi = E' \tag{18}$$

Using the angle-action formalism, we arrive at the integrable Hamiltonian with one degree of freedom, where E' is the total energy. This Hamiltonian satisfies the following equations:

$$\begin{cases} \dot{I} = -\dfrac{\partial \overline{H'}}{\partial \psi} = F\sqrt{2I}\cos\psi \\ \dot{\psi} = \dfrac{\partial \overline{H'}}{\partial I} = 2I - (\delta - k) - \dfrac{F}{\sqrt{2I}}\sin\psi \end{cases} \tag{19}$$

With (18) and (19) we can directly integrate the equations of motion and find fixed points. From (18) we have $\sin\psi = \dfrac{(I^2 - I\,(\delta - k)) - E'}{F\sqrt{2I}}$. With the first equation of the system (19) and after some algebra we obtain:

$$\zeta(I) = \int_{I_{min}}^{I} \frac{dI'}{\sqrt{2I'F^2 - [(I'^2 - I'\,(\delta - k) - E')]^2}} \tag{20}$$

Here the domain of convergence is given by $I \in]I_{min}, I_{Max}[$. This integral can be expressed in term of elliptic functions. In this way in the old variables we can obtain the parametric equation for the electron motion.

Another interesting application of (19) is the determination of fixed points (elliptic and hyperbolic). These points are defined by the equations: $\dot{I} = 0$ and $\dot{\psi} = 0$ (the forces are zero). From the first equation of (19) we have for $\dot{I} = 0$ two possibilities: $\psi_1 = \dfrac{\pi}{2}$ or $\psi_2 = \dfrac{3\pi}{2}$. For $\psi_1 = \pi/2$ the second equation of (19) gives:

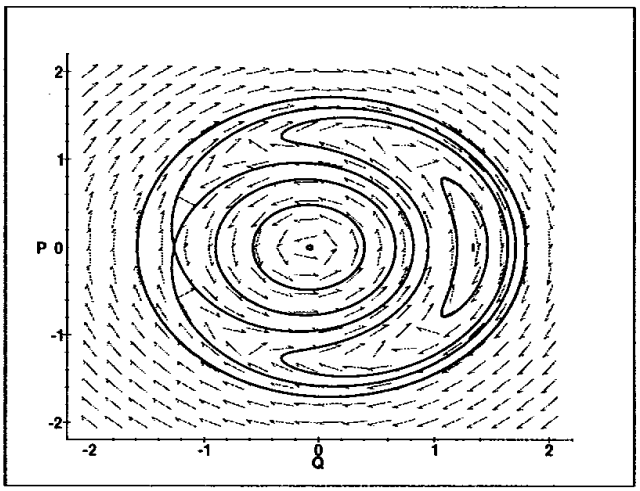

Figure 3: The phase portrait of (19) in the case of three real roots

$$2I - (\delta - k) - \frac{F}{\sqrt{2I}} = 0, \quad \text{where} \quad F \geq 0. \tag{21}$$

We have only one real root which corresponds to the elliptic point. For $\psi_1 = 3\pi/2$ the second equation of (19) becomes:

$$2I - (\delta - k) + \frac{F}{\sqrt{2I}} = 0, \quad \text{where} \quad F \geq 0. \tag{22}$$

If $F \leq \frac{2}{3\sqrt{3}}(\delta - k)^{3/2}$, we obtain two real roots, one of which is an elliptic point and the other one is a hyperbolic point. Depending on the value of F, the phase space will have either one, two, or three fixed points. When F increases the elliptic and hyperbolic points of (22) collide and disappear. Also the separatrix disappears (Hamiltonian bifurcation), see Fig.3.

It is possible to find the equation for separatrices of the hyperbolic point. It turns out to be the Pascal limacon. From the Hamiltonian (18) we have

$$I^2 - I(\delta - k) - F\sqrt{2I}\sin\psi = I_0^2 - I_0(\delta - k) + F\sqrt{2I_0} \tag{23}$$

where I_0 is a root of (22) corresponding to the hyperbolic point and $\psi_0 = 3\pi/2$. Let us introduce the new variables

$$I - I_0 = \sqrt{R}\left(\sqrt{R} - 2\sqrt{I_0}\sin\varphi\right),$$

$$\sqrt{I}\sin\psi + \sqrt{I_0} = \sqrt{R}\sin\varphi.$$

After some algebra we find

$$\sqrt{R}\left(\sqrt{R} - 2\sqrt{I_0}\sin\varphi\right)^2 + \sqrt{R}(2I_0 - \delta + k)$$
$$-\sqrt{2}\sin\varphi\left(F + (2I_0 - \delta + k)\sqrt{2I_0}\right) = 0$$

Since I_0 is the root of (22), we obtain the equation for the Pascal limacon

$$\left(\sqrt{R} - 2\sqrt{I_0}\sin\varphi\right)^2 = \delta - k - 2I_0. \tag{24}$$

The single elliptic point or central fixed point of (21) is always preserved. These results are in agreement with the results obtained in [3] by means of the mathematical analysis of the corresponding equations. However, using the angle-action formalism we have shown also that the Hamiltonian (6) with a periodic perturbing force in the form of trigonometric functions is completely integrable which means that no chaotic solutions exist, because for an integrable system the entire phase space is filled with invariant tori and any trajectory will remain on the particular torus selected by the initial conditions.

To illustrate in detail the location of the fixed points, we now present the Poincaré sections obtained by numerical integration of the dynamical system (5) for several sets of the control parameters. In Fig. 4 we show the results for $\Delta = -0.2$, $F = 0.01$ and $k = 1$. In this case there are three fixed points. With the help of (16), (22) and (23) we can accurately compute the positions of the elliptic and hyperbolic points in the phase space. There are two elliptic points located at $P_1 = 0$ and $Q_1 = 0.47038$ and at $P_2 = 0$ and $Q_2 = -0.05065$, and one hyperbolic point at $P_3 = 0$ and $Q_3 = -0.4197$. Fig. 5 illustrates the case ($F = 0.0333$) with the Hamiltonian bifurcation when the elliptic and hyperbolic points of (23) merge at $P_2 = 0$ and $Q_2 = -0.2582$ (double root), and the separatrix disappears. Fig. 6 shows for $\Delta = -0.2$, $F = 0.1$, and $k = 1$ one elliptic point of (22) at $P_1 = 0$ and $Q_1 = 0.6045$. The hyperbolic and elliptic points disappear, because (23) has no real roots.

It should be emphasized that in these three examples the parameter Δ was chosen to be negative which is not typical in gyrotrons operating in normal regimes. This was done solely for illustrative purposes, because as can be easily seen from Eq. (22) and the condition following it δ has to be larger than k. For $\Delta > 0$ we have only one central fixed point. For example, (see Fig. 7) for $\Delta = 0.5$, $F = 0.1$, and $k = 1$ the central fixed point is located at $P_1 = 0$ and $Q_1 = 0.12269$.

B. Realistic resonator

We now investigate the gyrotron equation in a completely realistic case when a resonator has a finite length and the perturbation (RF field) is an aperiodic

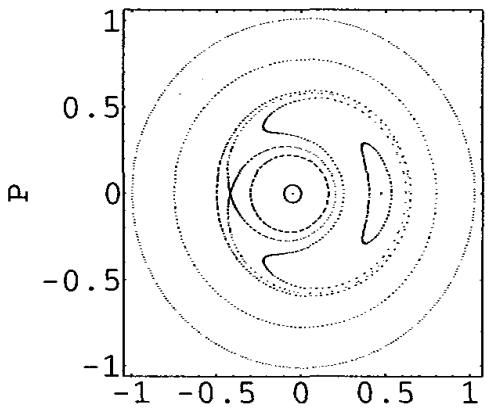

Figure 4: Poincare section with three fixed points ($\Delta = -0.2$, $F = 0.01$, and $k = 1$.)

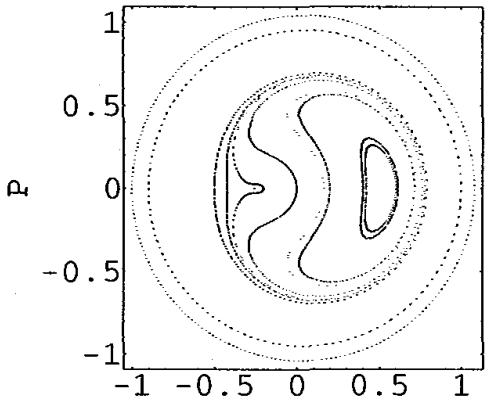

Figure 5: Poincare section with the Hamiltonian bifurcation. The elliptic and hyperbolic points merge at $P = 0$ and $Q = -0.2582$. ($\Delta = -0.2$, $F = 0.0333$, and $k = 1$).

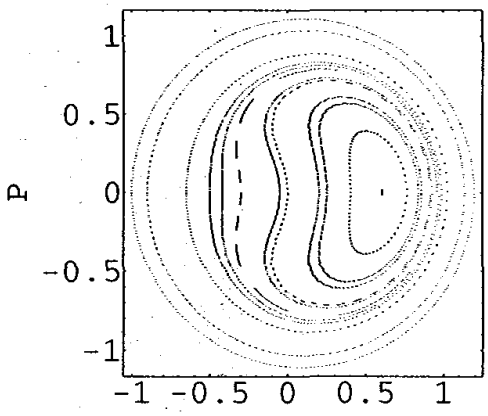

Figure 6: Poincare section with the central fixed point. ($\Delta = -0.2$, $F = 0.1$, and $k = 1$.)

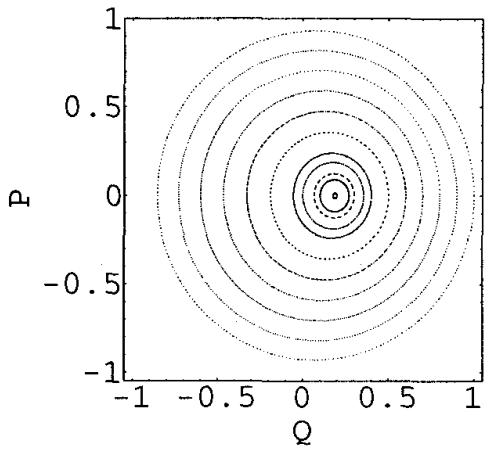

Figure 7: Poincare section with the central fixed point. ($\Delta = 0.5$, $F = 0.1$, and $k = 1$.)

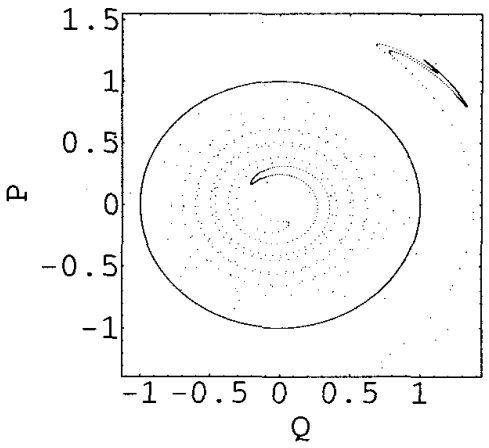

Figure 8: Phase space of 720 electrons after their passage through a resonator with RF field profile shown in Fig.1. Here $\mu \approx 9$, $F = 0.125$, $\Delta = 0.5$, and $\eta_\perp = 0.06$.

function for small ζ and an approximately periodic function for large ζ. The perturbation begins at $\zeta_{in} = 0$ and ends at $\zeta_{out} = 100$. Its form is shown in Fig. 1. For computational purposes we have interpolated this true function $f(\zeta)$ by a cubic spline. We integrate the dynamical system (5), which now is a nonhamiltonian system due to the finite interaction length, by means of the Runge-Kutta method with high accuracy to avoid the numerical noise. The transit time of the electron in a realistic resonator is very short and the motion is not bounded by the potential. For this reason we cannot use the Poincaré section to analyze correctly the solution of (5), because the number of points is not sufficient to construct the KAM tori for each initial condition. As a result, it is very difficult to say whether the solutions are chaotic or not. However, if we accept the fact that sensitive dependence of the solution of the system of differential equations on initial conditions is one of the definitions of chaos, we can try to detect a possible exponential divergence between the trajectories. For this purpose we have computed for the parameter values $\Delta = 0.5$ and $F = 0.125$ real trajectories of 720 electrons with different initial conditions Q_0 and P_0 distributed uniformly in $[0, 2\pi]$ on the unit circle defined by $\sqrt{Q_0^2 + P_0^2} = 1$. Fig. 8 shows the corresponding phase space of these electrons after their passage through the resonator.

Recall that the variables Q and P in our dynamical system represent the components of the dimensionless transverse momentum of the electron. Two distinct domains can be seen: the electrons beyond the unit circle have been accelerated and the electrons inside the unit circle have been decelerated. This means that for some particular initial conditions there should be a transition between the two kinds of motion. For almost all of the electrons the motion is never chaotic which means that for very close initial conditions the corresponding trajectories remain close. The trajectories may become sensitive with respect to the initial conditions in the vicinity of the transition points. To detect accurately these points, we show in Fig. 9 the transversal momentum at the resonator end as a function of the entrance angle. We observe three transition points: at $\sim$ 34, $\sim$ 70, and $\sim$ 187 degrees. The point at $\sim$ 34 is of special interest: in this region the electron is either strongly decelerated or accelerated. In Fig. 10 we show $|p|$ as a function of the initial angle within the sharp peak around 34 degrees. It is interesting to observe that the structure in this narrow region is very similar to the structure seen in Fig. 9. In a certain sense this self-similarity can be interpreted as a trace of chaos (fractal-dimensions). Moreover, in Figs. 11 and 12 we show in two and three dimensions respectively the motion of two electrons with very close entrance angles: 33.4 and 33.9 degrees. For the entrance angle equal to 33.4 degrees the electron is accelerated and it rotates always in the same direction. However, for the entrance angle equal to 33.9 degrees the electron is slowed down, and it changes its direction of rotation with respect to RF field. This change occurs when the electron travels through the region where the aperiodic part of $f(\zeta)$ becomes periodic. If we recall that sensitive dependence of the solutions on initial conditions is one of the definitions of chaos, we can conclude that in the vicinity of this entrance angle the trajectories of the electrons may become chaotic.

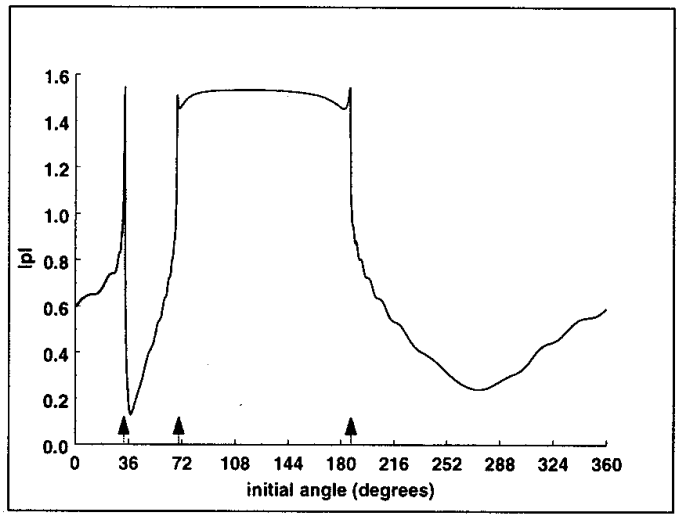

Figure 9: Transverse momentum of electrons at the resonator end as a function of the initial angle. Here $\mu \approx 9$, $F = 0.125$, $\Delta = 0.5$, and $\eta_\perp = 0.06$.

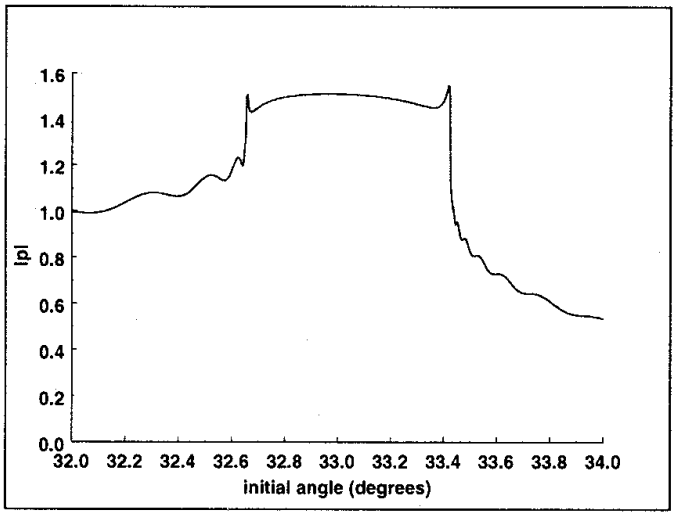

Figure 10: Same as Fig. 9, but in a narrow region around the first peak.

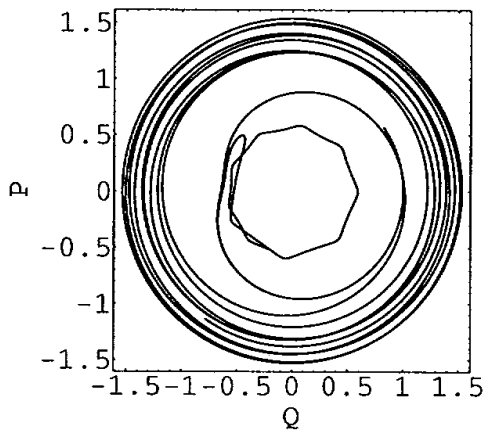

Figure 11: Two-dimensional trajectories of two electrons with close initial conditions: 33.4 and 33.9 degrees. The two trajectories begin at ($Q \approx 0.832; P \approx 0.554$) and diverge at ($Q \approx -0.6; P \approx 0.25$).

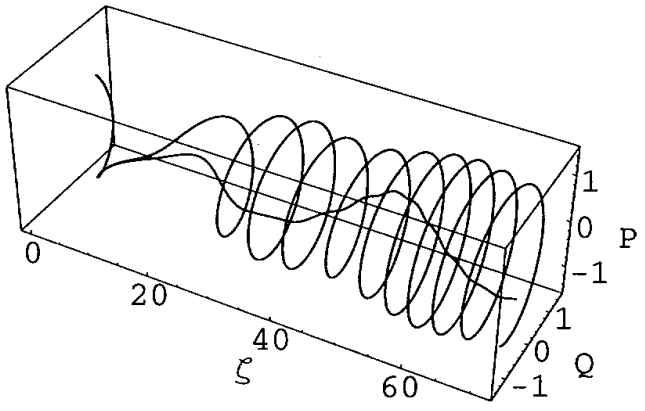

Figure 12: Same as Fig. 11 but in three dimensions.

IV. Efficiency plots.

The knowledge of the electron energy distribution at the exit from the interaction space (Fig. 9) is important in designing depressed collectors. For smooth distributions less stages of retarding potential are needed. The question arises about the correlation between the efficiency and smoothness which we define as follows:

$$S = \int_0^{2\pi} \left| \frac{dp(\zeta_{out})}{d\theta_0} \right| d\theta_0 \tag{25}$$

To illustrate this point, we have calculated for a realistic RF field profile with $\mu = 12.8$ efficiency, $\eta_\perp$, and smoothness, S, contours (Fig. 13). It is seen that generally the regions of high efficiencies and high smoothness (small S) overlap, albeit some compromise is possible. For example, in Fig. 14 we show energy distributions for three operating points: i) $\Delta = 0.55$, $F = 0.11$, $\eta_\perp = 0.78$, $S = 2.1$, ii) $\Delta = 0.35$, $F = 0.04$, $\eta_\perp = 0.34$, $S = 1.4$, iii) $\Delta = 0.35$, $F = 0.10$, $\eta_\perp \approx 0$, $S = 4.6$.

V. Concluding remarks

1. Using the powerful Hamiltonian method we have classified electron trajectories in an idealized gyrotron resonator (infinitely long and with an idealized force in the form of trigonometric functions). We have proved that in this case the system is fully integrable and that no chaotic motions are possible. This indirectly confirms the results of [4] who find no chaotic behavior of electron trajectories. They consider a plane traveling wave of constant amplitude as a force which practically corresponds to our case discussed in Sec. III A.

2. In real (finite) gyrotron resonators with a realistic strong aperiodic force we have found that the motion of the electrons in the vicinity of some particular initial angles is very sensitive with respect to the exact value of the initial angle. This sensitivity allows us to conclude that the trajectories of the electrons for these particular initial conditions may become chaotic. For other values of the control parameters μ, F, and Δ we can expect a similar chaos-like behavior in vicinities of other initial angles. In practical terms this means that there are electrons whose energy is unpredictable after they leave the interaction region. The larger the current, the larger is the number of such electrons.

3. For a specific value of $\mu = 12.8$ we have calculated efficiency and smoothness contours in the $\Delta - F$ plane and have found that the regions of high efficiencies in general coincide with the regions of high smoothness.

Acknowledgment

One of us (O.D.) expresses his gratitude to M.I. Petelin for useful remarks.

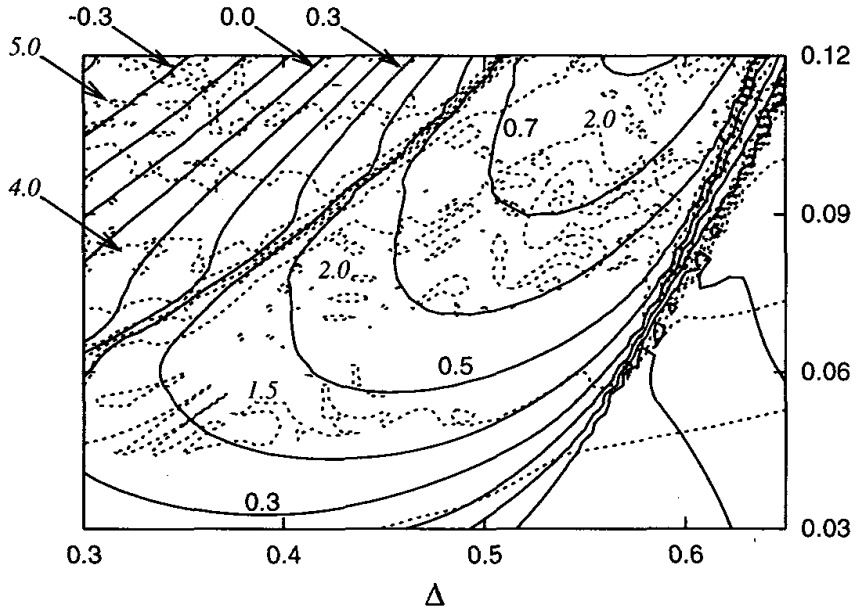

Figure 13: Efficiency (solid) and smoothness (dotted) contours calculated in the cold-cavity approximation with a realistic field profile with $\mu = 12.8$.

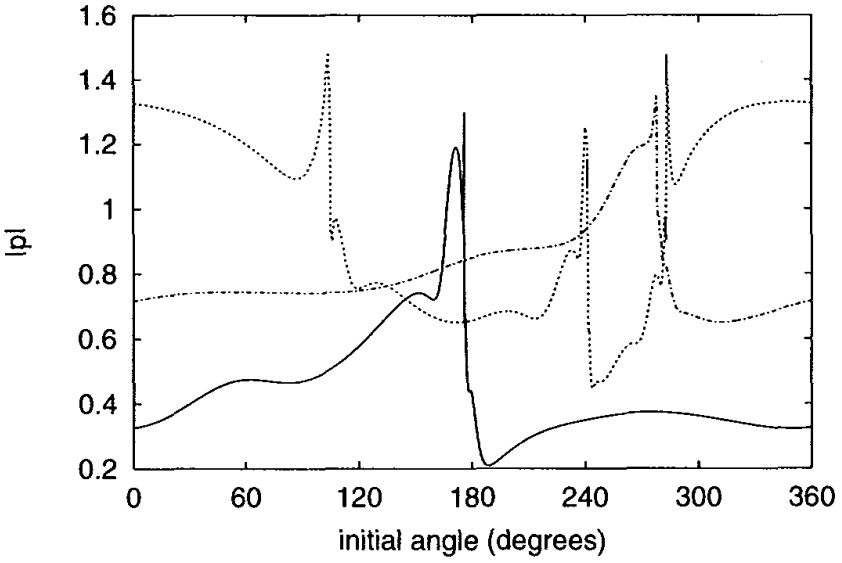

Figure 14: Transverse momentum of electrons at the resonator end as a function of the initial angle. Solid: $\Delta = 0.55$, $F = 0.11$, $\eta_\perp = 0.78$, $S = 2.1$. Dash-dot: $\Delta = 0.35$, $F = 0.04$, $\eta_\perp = 0.34$, $S = 1.4$. Dotted: $\Delta = 0.35$, $F = 0.10$, $\eta_\perp \approx 0$, $S = 4.6$

References

[1] *Gyrotron Oscillators. Their Principles and Practice,* C.J. Edgcombe, Ed. London, U.K.: Taylor & Francis, 1993.

[2] O. Dumbrajs, R. Meyer–Spasche, and A. Reinfelds, IEEE Trans. Plasma Sci. **26**, 846 (1998).

[3] O. Dumbrajs and A. Reinfelds, Mathematical Modeling and Analysis **3**, 74 (1998).

[4] P.A. Lindsay and X. Chen, IEEE Trans. Plasma Sci. **22**, 834 (1994).

[5] V.K. Yulpatov, "Reduced equations of autooscillations of a gyrotron" *Gyrotron*, Institute of Applied Physics, Academy of Sciences of the USSR, Gorky, 1981. Collection of scientific papers, Editor A.V. Gaponov-Grekhov, pp. 26-40.

[6] A.J. Lichtenberg and M.A. Lieberman, *Regular and Chaotic Dynamics.* New York, USA: Springer-Verlag, 1992.